Circ J 2006; **70:** 942–944

Intracoronary Injection of Granulocyte Colony-Stimulating Factor Ameliorates the Progression of Left Ventricular Remodeling After Myocardial Ischemia/Reperfusion in Rabbits

Hiroshi Hasegawa, MD; Hiroyuki Takano, MD; Hirokazu Shiraishi, MD; Kazutaka Ueda, MD; Yuriko Niitsuma, MD; Hiroyuki Tadokoro, MD; Issei Komuro, MD

Background Although granulocyte colony-stimulating factor (G-CSF) is known to prevent left ventricular (LV) remodeling after acute myocardial infarction (AMI), the best method of administration is unknown.
Methods and Results A rabbit ischemia/reperfusion model was created and G-CSF was administered into the coronary artery immediately after reperfusion. The LV size and contraction were determined by echocardiography, and the extent of infarcted myocardium was measured by Masson-Trichrome staining. The benefits of intracoronary injection of G-CSF on LV remodeling were similar to subcutaneous injection.
Conclusions Direct intracoronary G-CSF injection may become a new therapy for AMI with lower adverse effects. (*Circ J* 2006; **70:** 942–944)

Key Words: Granulocyte colony-stimulating factor; Ischemia/reperfusion; Remodeling

We and others have reported that granulocyte colony-stimulating factor (G-CSF) prevents left ventricular (LV) remodeling after acute myocardial infarction (AMI)[1–5] and improves limb ischemia[6] We recently demonstrated that it inhibits the progression of LV remodeling through direct activation of the Jak2/STAT3 pathway, which has anti-apoptotic effects and angiogenic effects[7] in cardiomyocytes. Because leukocytosis may have a deleterious effect on atherosclerosis and the infarcted myocardium, the most effective method of administrating G-CSF with less activation of bone marrow (BM) and more stimulation on cardiomyocytes is necessary. In the present study, we investigated the effects of direct intracoronary (IC) administration of G-CSF using a rabbit ischemia/reperfusion model.

Animal Models

The male Japanese white rabbit ischemia/reperfusion model was used[5] and all protocols were approved by the Institutional Animal Care and Use Committee of Chiba University. Under anesthesia, the carotid artery was cannulated with a 4-F wedge-pressure catheter and the tip of the catheter was placed at the supra-aortic valve. Next, left thoracotomy was performed and the large coronary arterial branch coursing down the middle of the anterolateral surface of the LV was ligated for 30 min. After release of the ligature, the ascending aorta was clamped by the balloon inflation of the wedge-pressure catheter and the rabbits were then randomized into 3 groups: (1) control group (CONT): saline injection into the coronary artery (n=12); (2) G-CSF IC group (IC): direct IC injection with recombinant human G-CSF (100μg/kg, rhG-CSF, Kirin Brewery Co Ltd, Tokyo, Japan, n=15) for 30 s; and (3) G-CSF SC group; subcutaneous (SC) injection of G-CSF (10μg/kg per day ×5 days, n=10).

Measurements

The number of circulating white blood cells (WBC) was measured at pre-operation and 1, 3, 5, 7 and 14 days after operation. Echocardiography was performed at pre-operation and 14 days after operation. At 14 days, rabbits were killed and the extent of infarcted myocardium in relation to total LV (%area) was measured by Masson-Trichrome staining.

Statistics

All measurements are expressed as group mean±SEM, and changes in cardiac function and infarct size were analyzed by 2-way repeated-measures ANOVA. Statistical differences were considered significant if the p-value was <0.05.

One CONT rabbit died during the study period, but none of the IC or SC rabbits (mortality rate; CONT: 6.6%; IC: 0%; SC: 0%) died. None of the groups showed loss of body weight or other behavioral problems. The number of WBC was more increased in the SC rabbits, and peaked at 7 days compared with the CONT rabbits, which peaked on day 1 (Table 1). In the IC rabbits, the WBC peak was on day 1 and decreased rapidly thereafter.

LV dilatation and dysfunction were less in the IC and SC rabbits than in CONT rabbits (Figs 1A,B). Although the area at risk measured by Evan blue staining was the same

(Received April 5, 2006; revised manuscript received May 12, 2006; accepted May 19, 2006)
Department of Cardiovascular Science and Medicine, Chiba University Graduate School of Medicine, Chiba, Japan
Mailing address: Issei Komuro, MD, Department of Cardiovascular Science and Medicine, Chiba University Graduate School of Medicine (M4), 1-8-1 Inohana, Chuo-ku, Chiba 260-8670, Japan. E-mail: komuro-tky@umin.ac.jp

Table 1 Number of WBCs in Peripheral Blood

	No. WBC (/μL)					
	Pre	*1 day*	*3 days*	*5 days*	*7 days*	*14 days*
CONT	*7,950±890*	*10,500±1,400*	*10,000±1,860*	*9,800±1,570*	*9,720±1,360*	*7,010±390*
IC	*7,720±360*	*21,450±2,860**	*12,910±2,580*	*13,010±2,070*	*12,180±1,670*	*7,200±400*
SC	*9,850±1,110*	*12,500±1,670*	*15,900±2,950**	*23,450±3,730**	*24,520±3,420**	*10,440±960**

*Results are mean±SEM. *p<0.05 vs CONT.*
WBC, white blood cell; CONT, control group; IC, intracoronary; SC, subcutaneous.

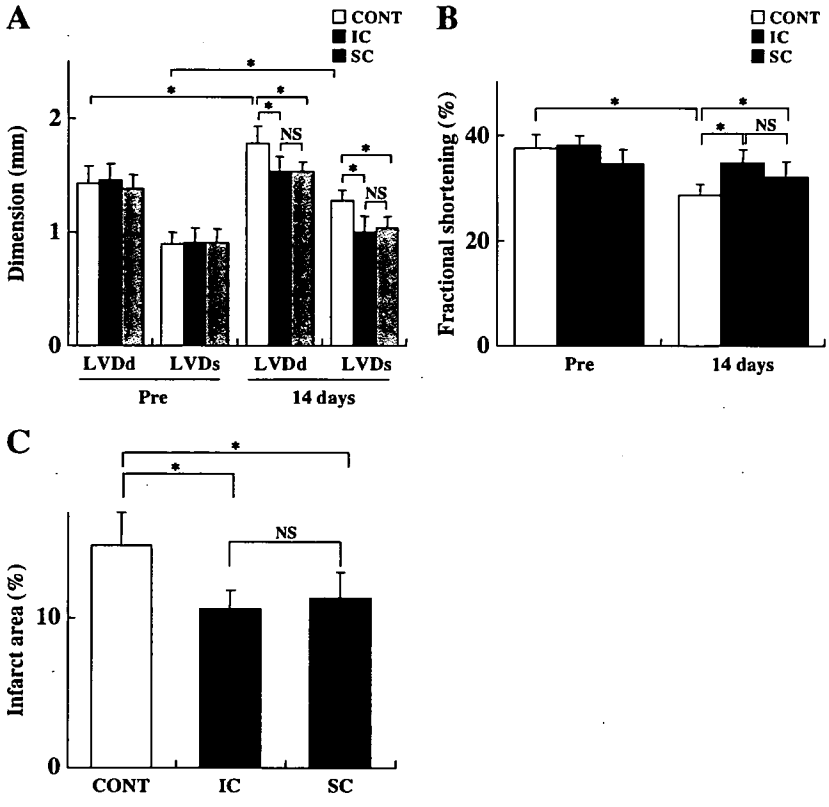

Fig 1. Effect of intracoronary granulocyte colony-stimulating factor (G-CSF) administration on (A) left ventricular end-diastolic diameter (LVDd) and end-systolic diameter (LVDs) and (B) left ventricular fractional shortening determined by echocardiography. (C) Effect of intracoronary G-CSF administration on myocardial infarction size measured by Masson-Trichrome staining. Results are expressed as mean±SEM. *p< 0.05. CONT, control group; IC, intracoronary; SC, subcutaneous.

in the 3 groups (CONT: 32.4±2.3%; IC: 35.7±2.6%; SC: 33.4±2.9%), the %area of infarcted myocardium was smaller in the IC and SC hearts compared with the CONT hearts (Fig 1C).

In this study using a rabbit ischemia/reperfusion model, one injection of G-CSF directly into the coronary artery prevented LV remodeling and reduced the infarct size by a degree similar to that with SC injection. Moreover the survival rate was also improved in relation to the inhibition of LV remodeling. Because the level of leucocytosis was less in the IC rabbits compared with the SC rabbits, the leucocytosis-induced systemic side effects are also thought to have been low.

The effects of G-CSF on the AMI-affected heart are mainly anti-apoptotic and angiogenetic through direct activation of the Jak2/STAT3 pathway in cardiomyocytes[2] In our previous study, the beneficial effects of G-CSF on LV remodeling were dose dependent and significantly reduced by a delayed start of treatment[2] Because the main effect of G-CSF on the AMI heart is the protection of cardiomyocytes, but not the mobilization of BM cells, earlier administration and a higher dose of G-CSF will conceivably protect cardiomyocytes more effectively after AMI. To more effectively protect infarcted myocardium with less systemic side effects, IC administration of G-CSF may be a better method of treating AMI.

Because most AMI patients are treated with percutaneous coronary intervention (PCI), it is very easy and reasonable to inject G-CSF into the coronary artery immediately after PCI. This treatment may become a new therapy for AMI patients and a more detailed study using large animals and a clinical study are awaited.

Acknowledgments

This work was supported by Health and Labour Sciences Research Grants, Uehara Memorial Foundation, Grant-in-Aid of The Japan Medical Association and Takeda Science Foundation.

References

1. Ohtsuka M, Takano H, Zou Y, Toko H, Akazawa H, Qin Y, et al. Cytokine therapy prevents left ventricular remodeling and dysfunction after myocardial infarction through neovascularization. *FASEB J* 2004; **18**: 851–853.
2. Harada M, Qin Y, Takano H, Minamino T, Zou Y, Toko H, et al.

G-CSF prevents cardiac remodeling after myocardial infarction by activating the Jak-Stat pathway in cardiomyocytes. *Nat Med* 2005; **11**: 305–311.
3. Takano H, Qin Y, Hasegawa H, Ueda K, Niitsuma Y, Ohtsuka M, et al. Effects of G-CSF on left ventricular remodeling and heart failure after acute myocardial infarction. *J Mol Med* 2006; **84**: 185–193.
4. Suzuki K, Nagashima K, Arai M, Uno Y, Misao Y, Takemura G, et al. Effect of granulocyte colony-stimulating factor treatment at a low dose but for a long duration in patients with coronary heart disease. *Circ J* 2006; **70**: 430–437.
5. Minatoguchi S, Takemura G, Chen XH, Wang N, Uno Y, Koda M, et al. Acceleration of the healing process and myocardial regeneration may be important as a mechanism of improvement of cardiac function and remodeling by postinfarction granulocyte colony-stimulating factor treatment. *Circulation* 2004; **109**: 2572–2580.
6. Ishida A, Ohya Y, Sakuda H, Ohshiro K, Higashiuesato Y, Nakaema M, et al. Autologous peripheral blood mononuclear cell implantation for patients with peripheral arterial disease improves limb ischemia. *Circ J* 2005; **69**: 1260–1265.

Angiotensin II Induces Premature Senescence of Vascular Smooth Muscle Cells and Accelerates the Development of Atherosclerosis via a p21-Dependent Pathway

Takeshige Kunieda, MD, PhD*; Tohru Minamino, MD, PhD*; Jun-ichiro Nishi, MD; Kaoru Tateno, MD, PhD; Tomomi Oyama, MD, PhD; Taro Katsuno; Hideyuki Miyauchi, MD, PhD; Masayuki Orimo, MD; Sho Okada, MD; Masayuki Takamura, MD, PhD; Toshio Nagai, MD, PhD; Shuichi Kaneko, MD, PhD; Issei Komuro, MD, PhD

Background—Angiotensin II (Ang II) has been reported to contribute to the pathogenesis of various human diseases including atherosclerosis, and inhibition of Ang II activity has been shown to reduce the morbidity and mortality of cardiovascular diseases. We have previously demonstrated that vascular cell senescence contributes to the pathogenesis of atherosclerosis; however, the effects of Ang II on vascular cell senescence have not been examined.

Methods and Results—Ang II significantly induced premature senescence of human vascular smooth muscle cells (VSMCs) via the p53/p21-dependent pathway in vitro. Inhibition of this pathway effectively suppressed induction of proinflammatory cytokines and premature senescence of VSMCs by Ang II. Ang II also significantly increased the number of senescent VSMCs and induced the expression of proinflammatory molecules and of p21 in a mouse model of atherosclerosis. Loss of p21 markedly ameliorated the induction of proinflammatory molecules by Ang II, thereby preventing the development of atherosclerosis. Replacement of *p21*-deficient bone marrow cells with wild-type cells had little influence on the protective effect of *p21* deficiency against the progression of atherogenesis induced by Ang II.

Conclusions—We demonstrated that Ang II promotes vascular inflammation by inducing premature senescence of VSMCs both in vitro and in vivo. Our results suggest a critical role of p21-dependent premature senescence of VSMCs in the pathogenesis of atherosclerosis. (***Circulation.*** **2006;114:953-960.)**

Key Words: aging ■ muscle, smooth ■ senescence

Aging is a physiological process associated with an increase in cardiovascular mobility and mortality even in the absence of known cardiovascular risk factors.[1] Age-associated changes in the blood vessels include a decrease in compliance and an increase in the inflammatory responses that promote atherogenesis.[2] It has been suggested that these alterations are attributable to age-related functional changes in vascular cells.[3–5] For example, endothelium-dependent vasodilation is impaired with age owing to decreased endothelial production of vasodilators such as nitric oxide (NO) and prostacyclin and to reduced responsiveness of vascular smooth muscle cells (VSMCs) to these vasodilators.[6] Adrenergic, endothelium-independent VSMC vasodilation also declines with age.[3] Moreover, increased expression of proinflammatory and prothrombogenic molecules was observed in vascular cells of aged arteries.[7] It is noteworthy that similar functional changes have been reported in senescent vascular cells in vitro.[8–11]

Clinical Perspective p 960

Cellular senescence is the limited ability of primary human cells to divide when cultured in vitro; it is accompanied by a specific set of phenotypic changes in morphology, gene expression, and function. These phenotypic changes have been suggested to have a role in human aging and age-associated diseases.[12] This hypothesis of cellular aging was established by Hayflick[13] and is supported by evidence that the replicative potential of primary cultured human cells is dependent on donor age and that the growth potential of cultured cells is well correlated with the mean maximum lifespan of the species of origin. The histology of the lesions of human atherosclerosis has been studied extensively, and these studies have demonstrated that there are vascular cells that exhibit the morphological features of cellular senescence.[14,15] These suggest the occurrence of cellular senes-

Received March 13, 2006; revision received July 5, 2006; accepted July 7, 2006.

From the Department of Cardiovascular Science and Medicine (T. Kunieda, T. M., J.-i.N., K.T., T.O., T. Katsuno, H.M., M.O., S.O., T.N., I.K.), Chiba University Graduate School of Medicine, Chiba, Japan, and Department of Gastroenterology (M.T., S.K.), Graduate School of Medicine, Kanazawa University, Kanazawa, Japan.

*Drs Kunieda and Minamino contributed equally to this work.

The online-only Data Supplement can be found with this article at http://circ.ahajournals.org/cgi/content/full/CIRCULATIONAHA.106.626606/DC1.

Correspondence to Issei Komuro, MD, PhD, Department of Cardiovascular Science and Medicine, Chiba University Graduate School of Medicine, 1-8-1 Inohana, Chuo-ku, Chiba 260-8670, Japan. E-mail komuro-tky@umin.ac.jp

Circulation **is available at http://www.circulationaha.org** **DOI: 10.1161/CIRCULATIONAHA.106.626606**

cence in vivo. Recently, this notion has been confirmed by cytochemical analysis in vivo with senescence-associated β-galactosidase (SA β-gal) activity, a biomarker for cellular senescence. SA β-gal–positive vascular cells were detected in rabbit carotid arteries subjected to vascular injury.[16] We and others have demonstrated SA β-gal–positive vascular cells in human atherosclerotic plaque of coronary arteries obtained from patients who had ischemic heart disease.[17,18] SA β-gal–positive cells were predominantly localized on atherosclerotic plaque, but no positive cells were observed in the internal mammary arteries from the same patients, in which atherosclerotic changes were minimally observed. In advanced plaque, SA β-gal–positive VSMCs were detected in the intima and, to a lesser extent, in the media.[19] SA β-gal–positive cells exhibit increased expression of p53 and $p21^{Waf1/Cip1}$, alternative markers for cellular senescence, in human atheroma, which suggests the further evidence of in vivo senescence. These cells also show impaired function, such as the decreased expression of endothelial NO synthase and the increased expression of proinflammatory molecules.[19] There is also evidence indicating that progressive telomere shortening, a biomarker of cellular aging, occurs in human blood vessels, which may be related to age-associated vascular diseases.[20,21] Thus, cellular senescence in vivo may contribute to the pathogenesis of vascular aging.

Arterial components of the angiotensin II (Ang II) signaling cascade increase with aging and contribute to the pathogenesis of atherosclerosis, whereas inhibition of Ang II activity has been shown to reduce the morbidity and mortality of cardiovascular disease.[7] Ang II signaling appears to play a critical role in regulating many of the stimuli and signals that govern vascular aging and atherogenesis; however, the mechanism underlying the deleterious effects of Ang II on the cardiovascular system is not yet fully understood. We previously reported that Ras activation induced vascular cell senescence and inflammation, and we suggested that vascular cell senescence might contribute to human atherogenesis.[19] Because Ang II is known to activate the Ras signaling pathway,[22,23] we hypothesized that Ang II may promote the development of atherosclerosis by inducing vascular cell senescence. In the present study, we demonstrate that Ang II promotes vascular inflammation by inducing premature senescence of VSMCs. Ang II induces premature senescence via the p53/p21-dependent pathway. Inhibition of this pathway effectively suppresses induction of the production of proinflammatory cytokines, as well as cellular senescence, and thereby prevents the development of atherosclerosis. These results disclose a novel role of Ang II in cardiovascular diseases and will provide insights into a novel treatment for atherosclerosis.

Methods

Cell Culture and Treatment

Primary cultured human aortic VSMCs were purchased from Cambrex (Walkersville, Md) and were grown according to the manufacturer's instructions. After cultures reached confluence in growth medium (SmGM-2, Cambrex), the cells were transferred to serum-free DMEM (Sigma-Aldrich, St. Louis, Mo) and incubated with Ang II (Sigma). Staining for SA β-gal was performed as described previously.[18] Briefly, the samples were incubated for 24 hours at 37°C in freshly prepared β-gal staining solutions (pH 6.0) containing 1 mg/mL 5-bromo-4-chrolo-3-indlyl β-D-galactopyranoside (X-gal), 5 mmol/L potassium ferrocyanide, 5 mmol/L potassium ferricyanide, 150 mmol/L NaCl, 2 mmol/L $MgCl_2$, 0.01% sodium deoxycholate, and 0.02% Nonidet-40. In some experiments, VSMCs were treated with olmesartan (Sankyo Co, Ltd, Tokyo, Japan), PD123319 (Sigma), or *N*-acetyl cysteine (NAC; Sigma).

Luciferase Assay

The reporter gene plasmid (1 μg) was transfected into VSMCs at 24 hours before the luciferase assay. The control vector encoding *Renilla* luciferase (0.1 μg) was cotransfected as an internal control. Then the luciferase assay was performed with a dual luciferase reporter assay system (Promega, Madison, Wis) according to the manufacturer's instructions. The expression vector encoding *p21* cDNA[24] was a gift from Dr B Vogelstein (Johns Hopkins University, Baltimore, Md). pPG13-Luc, the luciferase reporter gene containing the p53 binding sites, was also a gift from Dr Vogelstein. p55-A2-Luc, the luciferase reporter gene containing the κB binding sites, was a gift from Dr T Fujita (The Tokyo Metropolitan Institute of Medical Science, Tokyo, Japan).[25]

Experimental Animals

The animal experiments were approved by our institutional review board. *ApoE*-deficient mice (C57BL/6 background) and *p21*-deficient mice were obtained from the Jackson Laboratory (Bar Harbor, Me). The *p21*-deficient mice were backcrossed with wild-type C57BL/6 mice for 6 generations, whereas *apoE/p21*-deficient mice (C57BL/6 background) were generated by crossing *apoE*-deficient mice and *p21*-deficient mice. Animals were housed under a 12-hour light/dark cycle and fed a normal chow diet. Blood pressure was measured with a noninvasive tail-cuff system. Blood samples were obtained from the mice at the time of euthanasia. Mice (4 to 6 months old) were anesthetized by intraperitoneal injection of a mixture of ketamine 100 mg/kg and xylazine 5 mg/kg, and an osmotic minipump (Alzet model 2004, Durect Corp, Cupertino, Calif) was implanted to deliver Ang II subcutaneously at a dose of 1.44 $mg \cdot kg^{-1} \cdot d^{-1}$ for 4 weeks. After Ang II treatment, the mice were killed by cervical dislocation. The heart and aorta were removed after systemic perfusion with phosphate-buffered saline (PBS) for histological examination, zymography, and RNA analysis.

Statistical Analysis

Results are expressed as mean±SEM unless otherwise stated. Comparison of results between different groups was performed by 1-way ANOVA or 2-way ANOVA followed by the Scheffé post hoc test, or by a nonparametric Kruskal-Wallis test followed by a Dunn multiple comparison test, as indicated in the online Data Supplement. An unpaired Student *t* test was performed for single comparisons between groups. Survival was estimated with the Kaplan-Meier method. A log-rank test was used to compare survival between groups. Statistical significance was accepted at a value of $P<0.05$.

The authors had full access to the data and take full responsibility for its integrity. All authors have read and agree to the manuscript as written.

Results

Ang II Induces Premature Senescence In Vitro

To determine whether Ang II induces cellular senescence in vitro, we treated human VSMCs with Ang II for 3 days and then examined markers of cellular senescence. SA β-gal activity was significantly increased in Ang II–treated VSMCs compared with control cells (Figure 1A). Ang II also significantly increased the transcriptional activity of p53 compared with that in vehicle-treated cells, and its effect was dose dependent (Figure 1B). Moreover, expression of p21 and p53 was elevated in Ang II–treated VSMCs (Figure 1C). Because Ang II type 1 (AT_1)–specific inhibitor but not Ang II type 2

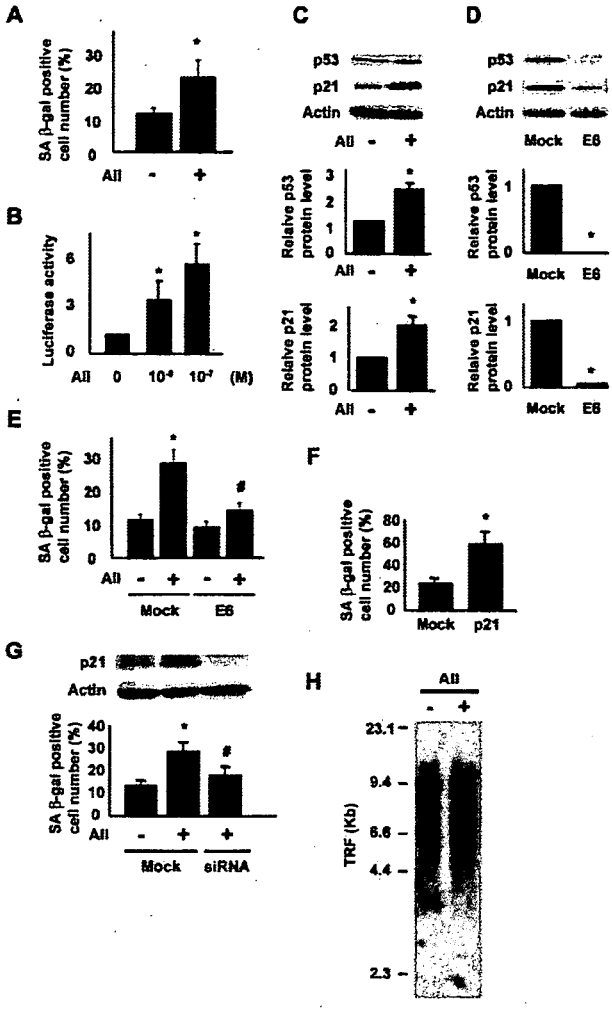

Figure 1. Ang II (indicated as AII) induces vascular cell senescence in vitro. A, After cultures reached confluence in growth medium, human VSMCs were transferred to serum-free medium and incubated with Ang II at a pathological concentration (10^{-7} mol/L) for 3 days. SA β-gal staining was performed as described in Methods, and the number of SA β-gal–positive cells was counted. *$P<0.05$ (unpaired t test, n=4). B, The luciferase reporter gene plasmid pPG13-Luc containing the p53-binding sequence was transfected into VSMCs, and the cells were treated with Ang II at the indicated concentration 24 hours before luciferase activity was measured. The activity of PG13-Luc in VSMCs treated with vehicle (Ang II=0) was designated as 1, and relative values were plotted. *$P<0.05$ vs Ang II=0 (1-way ANOVA, n=4). C, Whole-cell lysates (20 μg) were prepared from VSMCs treated with Ang II (+; 10^{-7} mol/L) or vehicle (−) for 3 days and were examined to detect expression of p53, p21, and actin (control) by Western blot analysis. Expression of p53 and p21 was standardized on the basis of actin expression, and the relative levels of expression are plotted in the graphs. The corrected value in vehicle-treated cells was designated as 1. *$P<0.05$ vs vehicle-treated cells (unpaired t test, n=5). D, VSMCs were infected with pBabe (Mock) or pBabe E6 (E6) and purified by culture with puromycin (0.8 μg/mL) for 3 days. The purified infected cells were then treated with Ang II (+) for 3 days, after which expression of p53, p21, and actin (control) was examined by Western blot analysis. Expression of p53 and p21 was standardized on the basis of actin expression, and the relative levels of expression are plotted in the graphs. *$P<0.05$ vs mock-infected cells (unpaired t test, n=5). E, VSMCs were infected as described for D and treated with Ang II (+) or vehicle (−) for 3 days, after which the number of SA β-gal–positive cells was counted. *$P<0.05$ vs Mock/Ang II (−), #$P<0.05$ vs Mock/Ang II (+; 2-way ANOVA, n=3). F, VSMCs were infected with pBabe (Mock) or pBabe p21 (p21) and purified by culture with puromycin (0.8 μg/mL) for 3 days. SA β-gal staining was performed, and the number of SA β-gal–positive cells was counted. *$P<0.05$ (unpaired t test, n=4). G, VSMCs were transfected with siRNA targeting p21 (p21) or random sequence (Mock) and treated with Ang II (+) or vehicle (−) for 3 days. SA β-gal staining was performed, and the number of SA β-gal–positive cells was counted. *$P<0.05$ vs Mock/Ang II(−), #$P<0.05$ vs Mock/Ang II (+; 1-way ANOVA, n=4). Western blot analysis verified p21 deletion by siRNA (upper panel). H, VSMCs were treated with Ang II (+) or vehicle (−) for 3 days. Genomic DNA was extracted, and telomere length was evaluated by Southern blot analysis as described in the Data Supplement (Methods). TRF indicates terminal restriction fragment.

(AT_2)–specific inhibitor significantly suppressed induction of p21 expression by Ang II treatment (Data Supplement, Figure I), it is likely that AT_1 mediates Ang II–induced senescence. To further investigate the relationship between Ang II and p53 transcription, we tested whether ablation of p53 could prevent Ang II–induced senescence. To do this, we infected VSMCs with a retroviral vector encoding the E6 oncoprotein of HPV16, which binds p53 and facilitates its destruction by ubiquitin-mediated proteolysis, or with an empty vector (mock infection). Western blot analysis revealed that introduction of E6 effectively reduced the level of p53 protein and also markedly reduced the expression of p21, its target protein (Figure 1D). Treatment of mock-infected VSMCs with Ang II significantly increased the number of SA β-gal–positive cells (Figure 1E). In contrast, the effect of Ang II on senescence was reduced in E6-infected VSMCs. We next examined the effect of p21 expression on Ang II–induced senescence. Overexpression of p21 significantly increased the number of SA β-gal–positive cells (Figure 1F), whereas p21 knockdown with a small interfering RNA (siRNA) system effectively blunted the effect of Ang II on senescence (Figure 1G). These results indicate a critical role of the p53/p21 pathway in Ang II–induced senescence.

Signals other than extended proliferation have been shown to result in cells developing a phenotype indistinguishable from that of senescent cells at the end of their replicative life span.[26] For example, the constitutive activation of mitogenic stimuli or oxidative stress induces a senescent phenotype. Cellular senescence triggered by such stimuli is independent of replicative age, and these signals act before the replicative limits of cells. Hence, it is apparently telomere-independent and thus is termed "stress-induced premature senescence." Ang II treatment induced cellular senescence within 3 days without telomere shortening (Figure 1H), which suggests that Ang II provokes stress-induced premature senescence.

Ang II Promotes Vascular Inflammation via the p53/p21-Dependent Pathway

It has been reported that Ang II causes vascular inflammation by upregulating the expression of various proinflammatory cytokines.[27–29] Because cellular senescence is also associated with the inflammatory response,[30] it is possible that Ang II promotes vascular inflammation via the p53/p21-dependent pathway. To test this notion, we examined the effects of E6 on Ang II–induced expression of proinflammatory cytokines. Expression of interleukin (IL)-1β by mock-infected VSMCs was increased after treatment with Ang II (Figure 2A), whereas this increase was effectively inhibited by introduc-

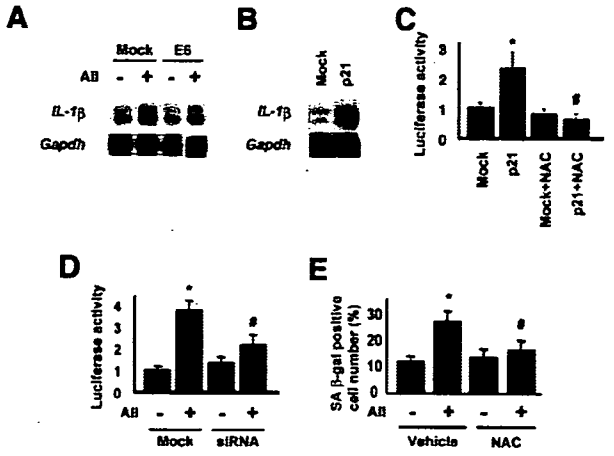

Figure 2. Ang II (indicated as AII) induces vascular inflammation in vitro. A, VSMCs were infected with pBabe (Mock) or pBabe E6 (E6) and purified by culture with puromycin (0.8 μg/mL) for 3 days. The purified infected cells were then treated with Ang II (+) or vehicle (−) for 3 days. Total RNA (10 μg) was extracted, and expression of *IL-1β* and *GAPDH* (control) was examined by the ribonuclease protection assay. Similar results were obtained from 3 independent experiments. B, VSMCs were infected with pBabe (Mock) or pBabe p21 (p21) and purified by culture with puromycin (0.8 μg/mL) for 3 days. Then, total RNA (10 μg) was prepared, and expression of *IL-1β* and *GAPDH* (control) was examined by the ribonuclease protection assay. Similar results were obtained from 3 independent experiments. C, The luciferase reporter gene plasmid containing the κB binding sites was transfected into VSMCs infected with pBabe (Mock) or pBabe p21 (p21), and cells were cultured in the absence or presence of NAC (0.5 mmol/L; +NAC). At 24 hours after transfection, luciferase activity was measured. The level of activity in mock-infected cells was designated as 1. **P*<0.05 vs Mock, #*P*<0.05 vs p21 (2-way ANOVA, n=6). D, VSMCs were transfected with siRNA targeting p21 (siRNA) or random sequences (Mock). Twenty-four hours after transfection, VSMCs were subsequently transfected with the luciferase reporter gene plasmid containing the κB binding sites and treated with Ang II (+) or vehicle (−). At 48 hours after siRNA transfection, luciferase activity was measured. The level of activity in mock-infected cells treated with vehicle was designated as 1. **P*<0.05 vs Mock/Ang II (−), #*P*<0.05 vs Mock/Ang II (+; 2-way ANOVA, n=5). E, VSMCs were cultured in the presence (+) or absence (−) of Ang II plus NAC (0.5 mmol/L) or vehicle for 3 days, after which the number of SA β-gal–positive cells was counted. **P*<0.05 vs Ang II (−)/Vehicle, #*P*<0.05 vs Ang II (+)/Vehicle (2-way ANOVA, n=4).

tion of E6 (Figure 2A). Overexpression of p21 markedly increased the expression of IL-1β compared with that in mock-infected cells (Figure 2B). Nuclear factor κB (NF-κB) is known to be one of the important transactivators of inflammatory cytokines.[27–29] To investigate whether overexpression of p21 led to an increase in NF-κB activity, a luciferase reporter gene containing NF-κB binding sites was introduced into p21-infected or mock-infected VSMCs. NF-κB activity was found to be significantly higher in p21-infected VSMCs than in mock-infected VSMCs (Figure 2C). Conversely, knockdown of p21 significantly inhibited NF-κB activation by Ang II treatment (Figure 2D). Overexpression of p21 in the absence of p53 increased NF-κB activity (Data Supplement, Figure II), which suggests that Ang II increases NF-κB activity by inducing p21 expression. It has been shown that p21 causes an increase of reactive oxygen species (ROS),[31] which can activate NF-κB. Therefore, we also examined the effect of an ROS scavenger, N-acetyl cysteine (NAC), on NF-κB activity. Enhancement of luciferase activity by p21 was significantly weaker in the presence of NAC (Figure 2C), which suggests that an increase of ROS mediated via p21 may be involved in Ang II–induced vascular inflammation. Moreover, NAC treatment effectively inhibited Ang II–induced senescence (Figure 2E).

Blood Pressure and Plasma Cholesterol Levels of *apoE*-Deficient Mice and *apoE/p21*-Deficient Mice 4 Weeks After Ang II Treatment

	ApoE KO	DKO	*P*
Blood pressure, mm Hg			
Before treatment	98.8±10.6	91.4±9.6	NS
After treatment	120.7±17.5	127.8±24.3	NS
Cholesterol, mg/dL	672.4±143.6	750.3±82.6	NS

ApoE KO indicates *apoE*-deficient mice; DKO, *apoE/p21*-deficient mice; and NS, no significant difference.

Values are expressed as mean±SEM (n=32).

Ang II Induces Cellular Senescence In Vivo

Next, we investigated whether Ang II could induce cellular senescence in vivo. We treated *apoE*-deficient mice with Ang II for 4 weeks and examined markers of cellular senescence in the vasculature. Consistent with our in vitro data, treatment with Ang II enhanced SA β-gal activity in the aortas of *apoE*-deficient mice (Figures 3A and 3B). Treatment of wild-type mice with Ang II did not markedly increase SA β-gal activity in the aortas (data not shown), and therefore, we focused on the effects of Ang II in *apoE*-deficient mice for further experiments. In *apoE*-deficient mice, most of the vascular cells that were positive for SA β-gal activity concomitantly exhibited immunoreactivity for α-smooth muscle actin (Figure 3A), which indicates that these were probably senescent VSMCs. Northern blot analysis revealed that aortic expression of p21 was markedly elevated by treatment with Ang II (Figure 3C). To further define the role of p21 in Ang II–induced senescence, we established *apoE/p21*-deficient mice and treated these animals with Ang II for 4 weeks. There were no differences in the blood pressure and lipid profiles between *apoE/p21*-deficient mice and *apoE*-deficient mice after Ang II treatment (Table). Disruption of *p21* did not significantly decrease SA β-gal–positive cells in the aorta of control *apoE*-deficient mice. In the Ang II–treated group, however, *apoE/p21*-deficient mice had significantly fewer SA β-gal–positive cells in the aorta than *apoE*-deficient mice (Figure 3B). To ascertain whether Ang II induces vascular inflammation via a p21-dependent pathway, we examined the aortic expression of various proinflammatory molecules. Ang II treatment strikingly induced the expression of proinflammatory cytokines, such as IL-1β and IL-6, as well as intercellular adhesion molecule-1 in the aortas of *apoE*-deficient mice, whereas *p21* deficiency effectively blocked the induction of these molecules by Ang II treatment (Figure 4A; Data Supplement, Figures III and IV). Likewise, Ang II markedly increased the aortic activity of matrix metalloproteinase-2 in *apoE*-deficient mice but not in *apoE/p21*-deficient mice (Figure 4B).

These results suggested that inhibition of vascular cell senescence might prevent the induction of atherosclerosis by

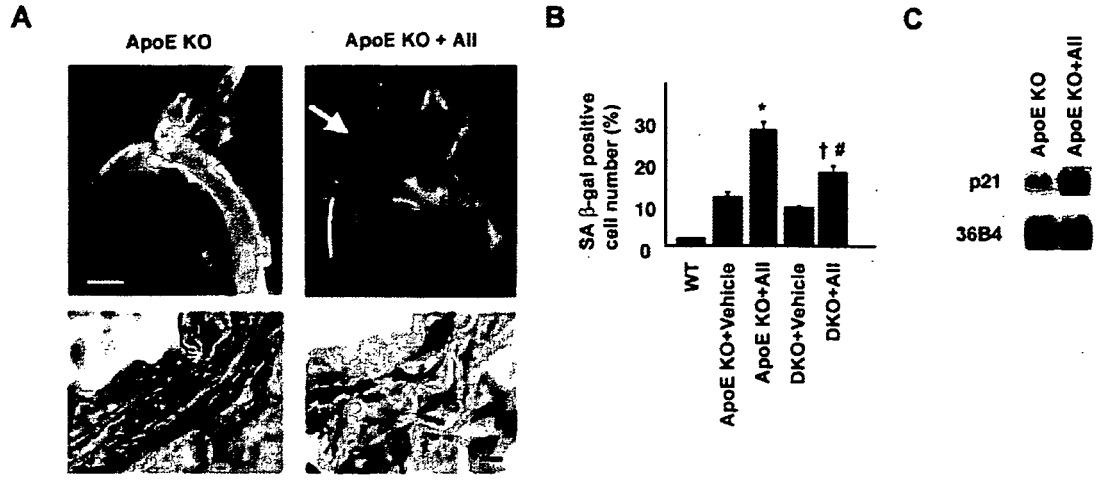

Figure 3. Ang II (indicated as AII) induces vascular cell senescence in vivo. A, *ApoE* knockout mice were treated with Ang II (1.44 mg · kg^{-1} · d^{-1}, ApoE KO+AII) or vehicle (ApoE KO) for 4 weeks. Then, the aortas were excised and subjected to SA β-gal staining (arrow, upper panel). Scale bar=1 mm. After the stained arteries were photographed, frozen sections were also prepared and stained with an antibody for α-smooth muscle actin (lower panel). Scale bar=50 μm. B, *ApoE* knockout mice (ApoE KO) and *apoE/p21* double-knockout mice (DKO) were treated with Ang II (+AII) or vehicle (+Vehicle) for 4 weeks. Untreated wild-type mice (WT) served as a control. The number of SA β-gal–positive VSMCs is shown relative to the total number of VSMCs. *$P<0.01$ vs ApoE KO+Vehicle, #$P<0.01$ vs ApoE KO+AII, †$P<0.01$ vs DKO+Vehicle (1-way ANOVA, n=10). C, Total RNA (30 μg) was extracted from the aortas of *apoE*-deficient mice treated with Ang II (ApoE KO+AII) or vehicle (ApoE KO) for 4 weeks, after which expression of *p21* and 36B4 (control) was examined by Northern blot analysis. Similar results were obtained from 3 independent experiments.

Ang II. It has already been reported that treatment with Ang II exacerbates atherogenesis in *apoE*-deficient mice and thereby promotes the formation of aortic aneurysms.[32,33] Consistent with such findings, we showed that Ang II treatment significantly increased the area of intimal thickening and the extent of aneurysm formation in the aortas of *apoE*-deficient mice (Figures 5A and 5B). The development of aortic aneurysms and atheroma after Ang II treatment was significantly less prominent in *apoE/p21*-deficient mice than in *apoE*-deficient mice (Figures 5A and 5B). Suppression of the induction of p21 by Ang II significantly increased the survival of these mice by preventing the rupture of aortic aneurysms (Figure 5C). Histological analysis revealed that the number of proliferating cell nuclear antigen–positive VSMCs in the intima of *apoE/p21*-deficient mice was greater than that of *apoE*-deficient mice (Data Supplement Figure V), which suggests that absence of p21 stabilizes atherosclerotic plaque. p21 has been reported to play a critical role in regulating the survival, proliferation, and differentiation of hematopoietic cells.[34–36] Because hematopoietic cells, especially macrophages, are involved in the process of atherosclerosis,[37] *p21* deficiency may affect macrophage proliferation

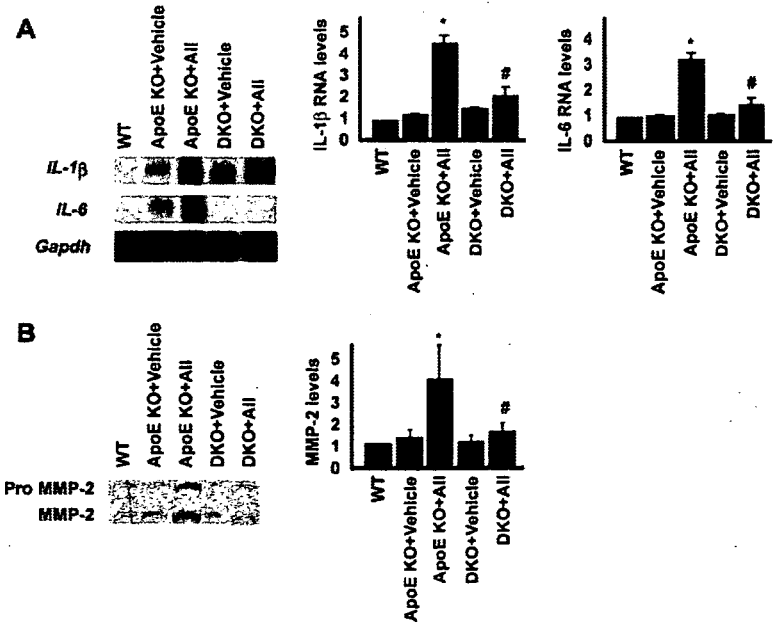

Figure 4. Ang II (indicated as AII) induces vascular inflammation in vivo. A, Ribonuclease protection assay for expression of *IL-1β* and *IL-6* in the aortas of *apoE*-deficient mice (ApoE KO) or *apoE/p21*-deficient mice (DKO) treated with Ang II (+AII) or vehicle (+Vehicle) for 4 weeks, or in the aortas of wild-type mice (WT). Expression of *IL-1β* and *IL-6* was standardized on the basis of *GAPDH* expression, and the relative levels of gene expression are plotted in the graph. The corrected value in wild-type mice was designated as 1. *$P<0.05$ vs ApoE KO+vehicle, #$P<0.05$ vs ApoE KO+AII (1-way ANOVA, n=5). B, Gelatin zymography for matrix metalloproteinase-2 (MMP-2) activity in the aortas of the same types of mice as in Figure 4A. The value in wild-type mice was designated as 1, and the relative levels of enzyme activity are plotted in the graph. *$P<0.05$ vs ApoE KO+vehicle, #$P<0.05$ vs ApoE KO+AII (1-way ANOVA, n=5).

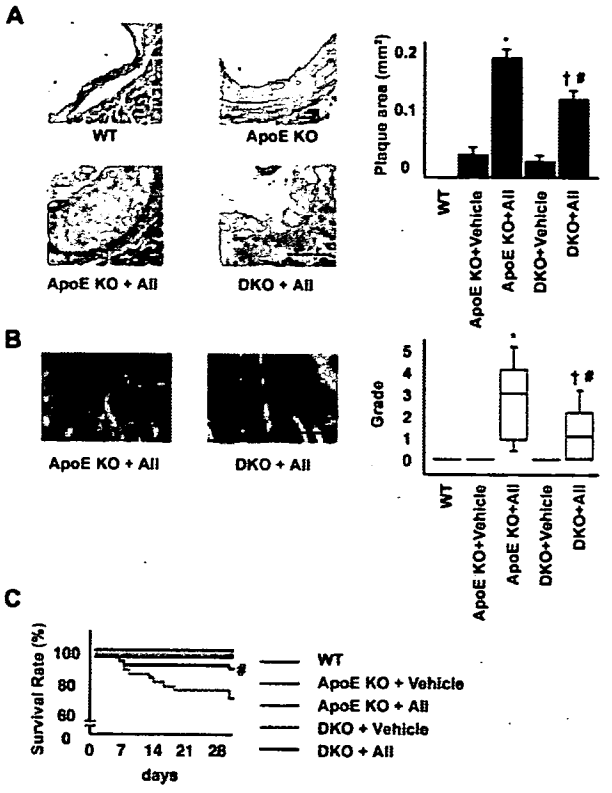

Figure 5. Ang II (indicated as AII) promotes the formation of aortic plaque and aortic aneurysms. A, *ApoE*-deficient mice (apoE KO) and *apoE/p21*-deficient mice (DKO) were treated with Ang II (+AII) or vehicle (+Vehicle) for 4 weeks. Untreated wild-type mice (WT) served as the control. The area of aortic plaque was evaluated as described in Methods. Scale bar=500 μm. *$P<0.01$ vs ApoE KO+Vehicle, #$P<0.05$ vs ApoE KO+AII, †$P<0.01$ vs DKO+Vehicle (1-way ANOVA, n=8). B, Aneurysm formation was graded as described in Methods. Results are shown as box plots, with median, 25th, and 75th percentiles represented as boxes, whereas the range is shown as bars. *$P<0.001$ vs ApoE KO+Vehicle, #$P<0.001$ vs ApoE KO+AII, †$P<0.01$ vs DKO+Vehicle (Kruskal-Wallis test, n=32). Ang II markedly promotes aneurysm formation in *apoE*-deficient mice but not in *apoE/p21*-deficient mice (left photographs). Scale bar=5 mm. C, The decreased survival of *apoE*-deficient mice treated with Ang II was reversed in *ApoE/p21*-deficient mice. #$P<0.05$ vs ApoE KO+AII (Kaplan-Meier method, n=32).

and thus protect against the promotion of atherogenesis by Ang II. To test this possibility, $apoE^{-/-}p21^{+/+}$ bone marrow cells were transplanted into *apoE/p21*-deficient or *apoE*-deficient mice that were then treated with Ang II for 4 weeks. Despite the transplantation of $apoE^{-/-}p21^{+/+}$ bone marrow, the number of SA β-gal–positive cells was still significantly lower in the aortas of *apoE/p21*-deficient mice than in *apoE*-deficient mice (Figure 6A). Likewise, the formation of aortic plaque was significantly inhibited in marrow-transplanted *apoE/p21*-deficient mice compared with marrow-transplanted *apoE*-deficient mice (Figure 6B), which suggests that p21 expression by vascular cells has a critical role in the development of atherosclerosis.

Discussion

Various mechanisms for the promotion of atherogenesis by Ang II have been suggested.[27–29] For example, Ang II is

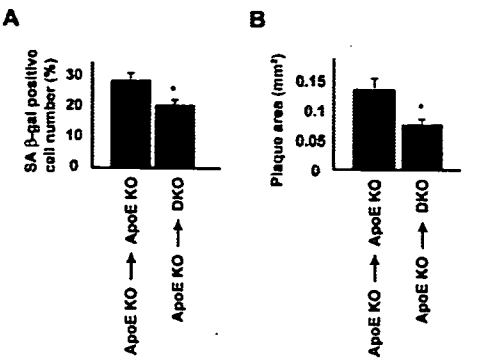

Figure 6. A dispensable role of p21 deficiency in bone marrow–derived cells in Ang II–induced atherogenesis. A, After bone marrow transplantation, *apoE*-deficient mice (ApoE KO→ApoE KO) and *apoE/p21*-deficient mice (ApoE KO→DKO) were treated with Ang II (indicated as AII) for 4 weeks. Our procedure for bone marrow transplantation provides chimeric mice with the chimeric rate being higher than 95%. The number of SA β-gal–positive VSMCs relative to the total number of VSMCs is shown. *$P<0.05$ vs ApoE KO→ApoE KO (unpaired *t* test, n=4). B, The aortic plaque area was evaluated in sections from each type of mouse mentioned in the legend to Figure 6A. *$P<0.05$ vs ApoE KO→ApoE KO (unpaired *t* test, n=4).

thought to increase the production of ROS and thereby activate several proinflammatory transcription factors such as NF-κB, thus leading to the onset of vascular inflammation and atherogenesis.[27,28] The present study showed that Ang II significantly induced vascular cell senescence and inflammation both in vitro and in vivo, with this induction being inhibited by the suppression of p21 expression. Ang II treatment prematurely provoked cellular senescence within 3 days without telomere shortening in vitro, which suggests that Ang II encourages stress-induced premature senescence. The protective effects of *p21* deficiency against Ang II–induced atherogenesis were preserved in *apoE/p21*-deficient mice even after transplantation with $p21^{+/+}$ bone marrow cells. Given these findings, we propose that Ang II induces vascular cell senescence and inflammation via a p21-dependent pathway, which may be one of the mechanisms underlying the promotion of atherogenesis by Ang II. Several enzymes have been implicated in the mechanism of vascular ROS formation mediated by Ang II, such as xanthine oxidase, cytochrome P450, uncoupled NO synthase, and nicotinamide adenine dinucleotide (NADH) oxidase.[38–40] The present in vitro data suggest that p21 activates proinflammatory transcription factors by increasing the production of ROS in vascular cells. It has been shown that cyclin-dependent kinase inhibitors, including p21, induce the expression of *PIG3*, a human homolog of the oxidoreductase genes of several species that increases the production of ROS.[31] Moreover, the signaling pathways of cyclin-dependent kinase inhibitors, it has been suggested, have a role in the activation of small G proteins that positively regulate NADH oxidase activity.[41] Collectively, these results suggest a critical role of p21 in the increase of vascular cell ROS formation provoked by Ang II.

We noted that the number of SA β-gal–positive cells was increased in the aortas of *apoE*-deficient mice compared with wild-type mice (Figures 3A and 3B). A small induction of proinflammatory molecules was also observed in the aortas of

apoE-deficient mice compared with wild-type mice, which likely contributes to the development of plaque formation (Figures 4A and 4B and Figure 5A). These results suggest that dyslipidemia also promotes vascular cell senescence and inflammation. Although *p21* deficiency significantly ameliorated Ang II–induced vascular cell senescence and inflammation, only a small effect of *p21* deficiency was observed in the vehicle-treated *apoE*-deficient mice (Figures 3A and 3B and Figures 4A and 4B), which suggests that dyslipidemia induces cellular senescence mainly via p21-independent pathways. Because loss of *p21* did not completely suppress the acceleration of atherogenesis by Ang II (Figures 5A and 5B), p21-independent pathways are also activated by Ang II treatment. We found that expression of $p16^{Ink4a}$ in the aortas of *apoE*-deficient mice was induced by Ang II treatment (Kunieda et al, unpublished data, 2006). Thus, both p53/p21- and p16-dependent pathways may be involved in Ang II–induced senescence and atherogenesis.

Merched and Chan[36] have recently reported that the absence of p21 protects against atherosclerosis in fat-fed *apoE*-deficient mice. Transplantation of *p21*-deficient bone marrow cells to wild-type mouse partially prevented the progression of atherosclerosis (32% reduction) compared with global p21 inactivation (52% reduction), which suggests that bone marrow–derived cells partially mediate the beneficial effects of p21 deficiency. Alternatively, other types of cells, such as vascular cells, likely mediate its effects to some extent. Consistent with the present study results, Merched and Chan's histological analyses of *apoE/p21*-deficient mice revealed a thicker and better-formed fibrous cap that consisted of VSMCs in atherosclerotic plaque than that found in *apoE*-deficient mice. Another recent study has demonstrated that the transcription factor Ets-1 is a critical regulator of Ang II–mediated vascular inflammation and remodeling in wild-type mice.[42] Although that study showed that Ang II treatment induced p21 expression via an Ets-1–dependent pathway, it remains unclear whether upregulation of p21 mediates Ang II–induced vascular inflammation and remodeling.

p53 immunoreactivity is present in vascular cells at sites of chronic inflammation in human arteries affected by atheroma, whereas only a few cells positive for p53 are found in control normal arteries.[43] p21 immunoreactivity is also detected in human atheroma but not in normal vessels, and it colocalizes with p53 immunoreactivity.[44] These observations suggest a pathological role of both p53 and p21 in human atherogenesis. It has been reported that atherosclerosis is aggravated in *p53/apoE*-deficient mice[45] and that macrophage p53 deficiency plays a critical role in the progression of atherosclerosis.[46] In contrast, a study using the perivascular collar model in *apoE*-deficient mice showed that overexpression of p53 results in a marked decrease of cell number and the extracellular matrix in cap lesions, leading to spontaneous plaque rupture.[47] In the present study, we demonstrated that suppression of p21 expression in the vasculature significantly reduced cellular senescence and the progression of atherosclerosis induced by Ang II. p21 deficiency stabilized atherosclerotic plaque by inhibiting vascular inflammation and inducing VSMC growth and thereby prevented plaque rupture. Thus, overexpression of p53 and p21 by vascular cells may have a deleterious effect in human atherosclerosis. Further studies on vascular cell senescence may provide novel insights into the clinical treatment of atherosclerosis.

Sources of Funding

This work was supported by a grant-in-aid for scientific research, developmental scientific research, and scientific research on priority areas from the Ministry of Education, Science, Sports, and Culture, and Health and Labor Sciences Research Grants (to Dr Komuro) and grants from Japan Research Foundation for Clinical Pharmacology, NOVARTIS foundation, and a grant-in-aid for scientific research from the Ministry of Education, Science, Sports, and Culture of Japan (to Dr Minamino).

Disclosures

None.

References

1. Lakatta EG, Levy D. Arterial and cardiac aging: major shareholders in cardiovascular disease enterprises: part I: aging arteries: a "set up" for vascular disease. *Circulation*. 2003;107:139–146.
2. Marin J. Age-related changes in vascular responses: a review. *Mech Ageing Dev*. 1995;79:71–114.
3. Cooper LT, Cooke JP, Dzau VJ. The vasculopathy of aging. *J Gerontol*. 1994;49:B191–B196.
4. Mombouli JV, Vanhoutte PM. Endothelial dysfunction: from physiology to therapy. *J Mol Cell Cardiol*. 1999;31:61–74.
5. Lakatta EG. Arterial and cardiac aging: major shareholders in cardiovascular disease enterprises: part III: cellular and molecular clues to heart and arterial aging. *Circulation*. 2003;107:490–497.
6. Brandes RP, Fleming I, Busse R. Endothelial aging. *Cardiovasc Res*. 2005;66:286–294.
7. Najjar SS, Scuteri A, Lakatta EG. Arterial aging: is it an immutable cardiovascular risk factor? *Hypertension*. 2005;46:454–462.
8. Matsushita H, Chang E, Glassford AJ, Cooke JP, Chiu CP, Tsao PS. eNOS activity is reduced in senescent human endothelial cells: preservation by hTERT immortalization. *Circ Res*. 2001;89:793–798.
9. Hoffmann J, Haendeler J, Aicher A, Rossig L, Vasa M, Zeiher AM, Dimmeler S. Aging enhances the sensitivity of endothelial cells toward apoptotic stimuli: important role of nitric oxide. *Circ Res*. 2001;89:709–715.
10. Nakajima M, Hashimoto M, Wang F, Yamanaga K, Nakamura N, Uchida T, Yamanouchi K. Aging decreases the production of PGI2 in rat aortic endothelial cells. *Exp Gerontol*. 1997;32:685–693.
11. Comi P, Chiaramonte R, Maier JA. Senescence-dependent regulation of type 1 plasminogen activator inhibitor in human vascular endothelial cells. *Exp Cell Res*. 1995;219:304–308.
12. Faragher RG, Kipling D. How might replicative senescence contribute to human ageing? *Bioessays*. 1998;20:985–991.
13. Hayflick L. Current theories of biological aging. *Fed Proc*. 1975;34:9–13.
14. Burrig KF. The endothelium of advanced arteriosclerotic plaques in humans. *Arterioscler Thromb*. 1991;11:1678–1689.
15. Ross R, Wight TN, Strandness E, Thiele B. Human atherosclerosis, I: cell constitution and characteristics of advanced lesions of the superficial femoral artery. *Am J Pathol*. 1984;114:79–93.
16. Fenton M, Barker S, Kurz DJ, Erusalimsky JD. Cellular senescence after single and repeated balloon catheter denudations of rabbit carotid arteries. *Arterioscler Thromb Vasc Biol*. 2001;21:220–226.
17. Vasile E, Tomita Y, Brown LF, Kocher O, Dvorak HF. Differential expression of thymosin beta-10 by early passage and senescent vascular endothelium is modulated by VPF/VEGF: evidence for senescent endothelial cells in vivo at sites of atherosclerosis. *FASEB J*. 2001;15:458–466.
18. Minamino T, Miyauchi H, Yoshida T, Ishida Y, Yoshida H, Komuro I. Endothelial cell senescence in human atherosclerosis: role of telomere in endothelial dysfunction. *Circulation*. 2002;105:1541–1544.
19. Minamino T, Yoshida T, Tateno K, Miyauchi H, Zou Y, Toko H, Komuro I. Ras induces vascular smooth muscle cell senescence and inflammation in human atherosclerosis. *Circulation*. 2003;108:2264–2269.
20. Chang E, Harley CB. Telomere length and replicative aging in human vascular tissues. *Proc Natl Acad Sci U S A*. 1995;92:11190–11194.

21. Ogami M, Ikura Y, Ohsawa M, Matsuo T, Kayo S, Yoshimi N, Hai E, Shirai N, Ehara S, Komatsu R, Naruko T, Ueda M. Telomere shortening in human coronary artery diseases. *Arterioscler Thromb Vasc Biol.* 2004; 24:546–550.
22. Eguchi S, Inagami T. Signal transduction of angiotensin II type 1 receptor through receptor tyrosine kinase. *Regul Pept.* 2000;91:13–20.
23. Berk BC, Corson MA. Angiotensin II signal transduction in vascular smooth muscle: role of tyrosine kinases. *Circ Res.* 1997;80:607–616.
24. el-Deiry WS, Tokino T, Velculescu VE, Levy DB, Parsons R, Trent JM, Lin D, Mercer WE, Kinzler KW, Vogelstein B. WAF1, a potential mediator of p53 tumor suppression. *Cell.* 1993;75:817–825.
25. Fujita T, Nolan GP, Liou HC, Scott ML, Baltimore D. The candidate proto-oncogene bcl-3 encodes a transcriptional coactivator that activates through NF-kappa B p50 homodimers. *Genes Dev.* 1993;7:1354–1363.
26. Serrano M, Blasco MA. Putting the stress on senescence. *Curr Opin Cell Biol.* 2001;13:748–753.
27. Cheng ZJ, Vapaatalo H, Mervaala E. Angiotensin II and vascular inflammation. *Med Sci Monit.* 2005;11:RA194–RA205.
28. Suzuki Y, Ruiz-Ortega M, Lorenzo O, Ruperez M, Esteban V, Equido J. Inflammation and angiotensin II. *Int J Biochem Cell Biol.* 2003;35: 881–900.
29. Brasier AR, Recinos A III, Eledrisi MS. Vascular inflammation and the renin-angiotensin system. *Arterioscler Thromb Vasc Biol.* 2002;22: 1257–1266.
30. Minamino T, Miyauchi H, Yoshida T, Tateno K, Kunieda T, Komuro I. Vascular cell senescence and vascular aging. *J Mol Cell Cardiol.* 2004; 36:175–183.
31. Macip S, Igarashi M, Fang L, Chen A, Pan ZQ, Lee SW, Aaronson SA. Inhibition of p21-mediated ROS accumulation can rescue p21-induced senescence. *EMBO J.* 2002;21:2180–2188.
32. Daugherty A, Manning MW, Cassis LA. Angiotensin II promotes atherosclerotic lesions and aneurysms in apolipoprotein E-deficient mice. *J Clin Invest.* 2000;105:1605–1612.
33. Daugherty A, Cassis LA. Mouse models of abdominal aortic aneurysms. *Arterioscler Thromb Vasc Biol.* 2004;24:429–434.
34. Cheng T, Rodrigues N, Shen H, Yang Y, Dombkowski D, Sykes M, Scadden DT. Hematopoietic stem cell quiescence maintained by p21cip1/waf1. *Science.* 2000;287:1804–1808.
35. Marone M, Bonanno G, Rutella S, Leone G, Scambia G, Pierelli L. Survival and cell cycle control in early hematopoiesis: role of bcl-2, and the cyclin dependent kinase inhibitors P27 and P21. *Leuk Lymphoma.* 2002;43:51–57.
36. Merched AJ, Chan L. Absence of p21Waf1/Cip1/Sdi1 modulates macrophage differentiation and inflammatory response and protects against atherosclerosis. *Circulation.* 2004;110:3830–3841.
37. Lusis AJ. Atherosclerosis. *Nature.* 2000;407:233–241.
38. Cai H, Harrison DG. Endothelial dysfunction in cardiovascular diseases: the role of oxidant stress. *Circ Res.* 2000;87:840–844.
39. Fleming I. Cytochrome p450 and vascular homeostasis. *Circ Res.* 2001; 89:753–762.
40. Griendling KK, Minieri CA, Ollerenshaw JD, Alexander RW. Angiotensin II stimulates NADH and NADPH oxidase activity in cultured vascular smooth muscle cells. *Circ Res.* 1994;74:1141–1148.
41. McAllister SS, Becker-Hapak M, Pintucci G, Pagano M, Dowdy SF. Novel p27(kip1) C-terminal scatter domain mediates Rac-dependent cell migration independent of cell cycle arrest functions. *Mol Cell Biol.* 2003;23:216–228.
42. Zhan Y, Brown C, Maynard E, Anshelevich A, Ni W, Ho IC, Oettgen P. Ets-1 is a critical regulator of Ang II-mediated vascular inflammation and remodeling. *J Clin Invest.* 2005;115:2508–2516.
43. Ihling C, Haendeler J, Menzel G, Hess RD, Fraedrich G, Schaefer HE, Zeiher AM. Co-expression of p53 and MDM2 in human atherosclerosis: implications for the regulation of cellularity of atherosclerotic lesions. *J Pathol.* 1998;185:303–312.
44. Ihling C, Menzel G, Wellens E, Monting JS, Schaefer HE, Zeiher AM. Topographical association between the cyclin-dependent kinases inhibitor P21, p53 accumulation, and cellular proliferation in human atherosclerotic tissue. *Arterioscler Thromb Vasc Biol.* 1997;17:2218–2224.
45. Guevara NV, Kim HS, Antonova EI, Chan L. The absence of p53 accelerates atherosclerosis by increasing cell proliferation in vivo. *Nat Med.* 1999;5:335–339.
46. Merched AJ, Williams E, Chan L. Macrophage-specific p53 expression plays a crucial role in atherosclerosis development and plaque remodeling. *Arterioscler Thromb Vasc Biol.* 2003;23:1608–1614.
47. von der Thusen JH, van Vlijmen BJ, Hoeben RC, Kockx MM, Havekes LM, van Berkel TJ, Biessen EA. Induction of atherosclerotic plaque rupture in apolipoprotein E-/- mice after adenovirus-mediated transfer of p53. *Circulation.* 2002;105:2064–2070.

CLINICAL PERSPECTIVE

Vascular cells have a finite lifespan when cultured in vitro and eventually enter an irreversible growth arrest called "cellular senescence." We previously demonstrated the presence of senescent vascular cells in human atherosclerotic lesions but not in nonatherosclerotic lesions. Moreover, these cells express increased levels of proinflammatory molecules and decreased levels of endothelial nitric oxide synthase, which suggests that cellular senescence contributes to the pathogenesis of human atherosclerosis. Angiotensin II (Ang II) has been reported to contribute to the pathogenesis of various human diseases, including atherosclerosis, and inhibition of Ang II activity has been shown to reduce the morbidity and mortality of cardiovascular diseases. Various mechanisms for the promotion of atherogenesis by Ang II have been suggested. Here, we report exciting new findings to show that Ang II promotes vascular inflammation by inducing vascular cell senescence. Ang II induces cellular senescence via a p53/p21-dependent pathway. Inhibition of this pathway effectively suppresses induction of the production of proinflammatory cytokines, as well as cellular senescence, by Ang II and thereby prevents the development of atherosclerosis. Our findings will provide insights into a novel treatment for atherosclerosis. Antisenescence would be a useful strategy for protection against age-associated vascular diseases.

Correction

In the article, "Angiotensin II Induces Premature Senescence of Vascular Smooth Muscle Cells and Accelerates the Development of Atherosclerosis via a p21-Dependent Pathway" by Kunieda et al that was published in the August 29, 2006, issue of the journal (*Circulation.* 2006;114:953–960), Figure 2C and Figure 2D were reversed. The corrected figure is in the current online version. The authors regret this error.

DOI: 10.1161/CIRCULATIONAHA.106.178461

(*Circulation.* 2006;114:e510.)

***Circulation* is available at http://www.circulationaha.org** **DOI: 10.1161/CIRCULATIONAHA.106.178461**

Original Article

Amelioration of Hypertensive Heart Failure by Amlodipine May Occur *via* Antioxidative Effects

Hiroshi HASEGAWA[1], Hiroyuki TAKANO[1], Takahide KOHRO[2], Kazutaka UEDA[1], Yuriko NIITSUMA[1], Hiroyuki ABURATANI[2], and Issei KOMURO[1]

Although recent clinical studies have suggested that long-acting calcium channel blockers (CCBs) have beneficial effects on heart failure, the precise mechanism is unknown. In this study, Dahl salt-sensitive rats fed a high salt diet were treated with the long-acting CCB amlodipine, the low-molecular-weight membrane permeable superoxide dismutase mimetic 4-hydroxy-2,2,6,6-tetramethyl piperidinoxyl (Tempol), or saline from 11 weeks after birth. The cardiac geometry and function, and gene expression profiles were determined at 17 weeks. Dahl salt-sensitive rats fed a high salt diet followed by saline as a non-treatment control (HS group) showed a marked increase in blood pressure and developed concentric hypertrophy at 11 weeks, followed by left ventricular (LV) dilation and congestive heart failure by 17 weeks. The treatment with amlodipine (AMLO group) or Tempol (TEMP group) significantly inhibited the development of LV hypertrophy and cardiac dysfunction. Analysis using an Affymetrix GeneChip U34 revealed that the expression levels of 195 genes were changed by the treatment with amlodipine. Among these 195 genes, 110 genes were increased in HS rats and decreased in AMLO rats. And of these 110 genes, 54 genes were also decreased in TEMP rats. In contrast, 85 genes were decreased in HS rats and increased in AMLO rats. Of these 85 genes, 38 genes were also increased in TEMP rats. Approximately 48% of the genes were changed in similar fashion in AMLO and TEMP rats, suggesting that amlodipine shows beneficial effects on heart failure mainly *via* antioxidative mechanisms. (*Hypertens Res* 2006; 29: 719–729)

***Key Words*: amlodipine, Dahl rat, gene chip, heart failure, hypertension**

Introduction

Hemodynamic overload, which can take the form of pressure or volume overload, causes left ventricular (LV) hypertrophy as an adaptive mechanism. However, sustained cardiac hypertrophy induces a reduction of contractile ability and/or a decrease in the number of viable myocytes, resulting in congestive heart failure (CHF) (*1–4*). It is very important to elucidate the molecular mechanism of the progression from cardiac hypertrophy to heart failure (*5*).

Calcium channel blockers (CCBs) are widely used to treat patients with hypertension (*6*), but treatment with short-acting CCBs has been reported to increase the risk of cardiovascular death, at least partly due to activation of the sympathetic nervous system (*7–9*). However, CCBs with an intrinsically long duration of activity have been shown to significantly reduce vascular resistance properties without significant effects on myocardial contractility (*10*). In the ACTION (A Coronary disease Trial Investigating Outcome with Nifedipine GITS [gastro-intestinal therapeutic system]) trial, the addition of long-acting nifedipine to conventional treatment of stable

From the [1]Department of Cardiovascular Science and Medicine, Chiba University Graduate School of Medicine, Chiba, Japan; and [2]Genome Science Division, Research Center for Advanced Science and Technology, University of Tokyo, Tokyo, Japan.

This work was supported by Health and Labour Sciences Research Grants, by a Grant-in-Aid from the Japan Medical Association, and by the Takeda Medical Research Foundation, the Uehara Memorial Foundation, the Kato Memorial Trust for Nambyo Research, and the Takeda Science Foundation.

Address for Reprints: Issei Komuro, M.D., Ph.D., Department of Cardiovascular Science and Medicine, Chiba University Graduate School of Medicine (M4), 1–8–1 Inohana, Chuo-ku, Chiba 260–8670, Japan. E-mail: komuro-tky@umin.ac.jp

Received January 24, 2006; Accepted in revised form May 29, 2006.

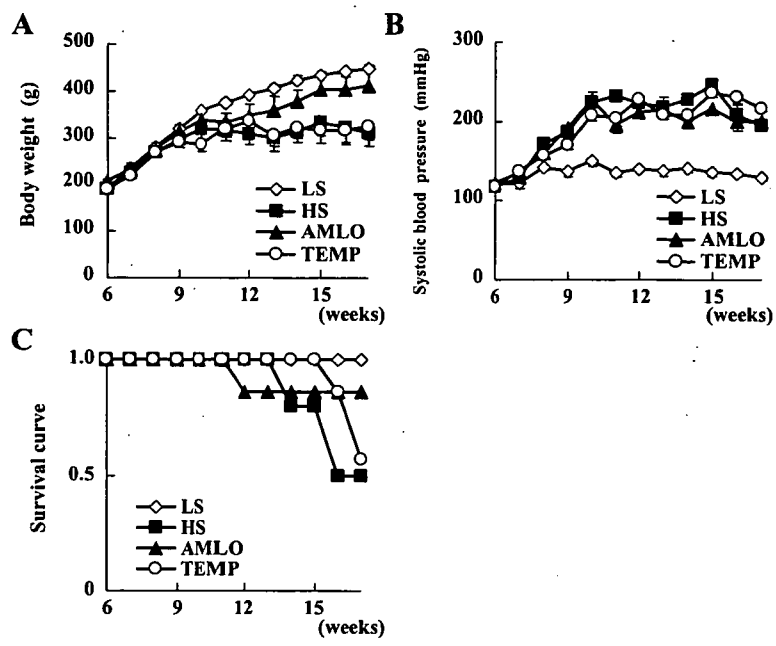

Fig. 1. *The change of blood pressure, body weight and mortality. A: The time course of body weight in LS, HS, AMLO and TEMP rats. Data are expressed as the mean±SEM (n = 10, 10, 7, 7, respectively). B: The time course of systolic blood pressure (SBP) in LS, HS and AMLO rats. Data are expressed as the mean±SEM (n = 10, 10, 7, 7, respectively). C: The time course of survival rate in LS, HS and AMLO rats (n = 10, 10, 7, 7, respectively).*

angina patients reduced the development of heart failure by 29% (*11*, *12*).

Amlodipine, a third generation dihydropyridine CCB, has much higher affinity for lipid constituents of the cellular membrane than do other CCBs (*13*). There are increasing basic and clinical data indicating that amlodipine and other CCBs, in addition to having hemodynamic properties, exert non–calcium channel-related pleiotropic actions, such as the release of nitric oxide (*14*), inhibition of adhesion molecules (*15*) and inhibition of matrix metalloproteinase-1 (*16*). Moreover, amlodipine inhibits cytokine-induced endothelial cell toxicity and has a potent membrane antioxidant activity independent of its calcium channel modulation (*17*). To determine whether amlodipine prevents the progression from hypertrophy to heart failure, we used a Dahl rat hypertensive heart failure model (*18–22*), and to gain insight into the underlying mechanisms of the effects of amlodipine, we performed DNA chip analysis (*23*, *24*).

Methods

Animals

Five-week-old male Dahl salt-sensitive rats (DS) were obtained from SLC (Shizuoka, Japan). All rats were housed in climate-controlled metabolic cages with a 12:12-h light-dark cycle. Twenty-four rats were fed a diet containing 0.3% NaCl until the age of 6 weeks, then fed a diet containing 8% NaCl (MF; Oriental Yeast, Tokyo, Japan) from 6 weeks of age until the end of the experiment. Seven of these 24 rats were then given amlodipine (10 mg/kg/day) by gavage once a day from 11 weeks to 17 weeks (AMLO group), 7 were given the low–molecular-weight membrane permeable superoxide dismutase (SOD) mimetic, 4-hydroxy-2,2,6,6-tetramethyl piperidinoxyl (Tempol; 10 mg/kg/day), by gavage once a day from 11 weeks to 17 weeks (TEMP group) and 10 rats were treated with saline as a non-treatment control (HS group). In addition, 10 rats were fed a diet containing 0.3% NaCl throughout this experiment as a normal blood pressure control (LS group). The blood pressure (BP) and body weight (BW) of all animals were measured every week. The peak systolic pressure was recorded by a photoelectric pulse device (Softron BP-98A; Softron Co., Tokyo, Japan) placed on the tail of unanesthetized rats as described previously (*25*). At 17 weeks of age, all DS rats with or without CHF were sacrificed, before their natural death, when signs of CHF such as rapid and labored respiration and LV diffuse hypokinesis on echocardiography were observed.

Throughout the studies, all animals were treated humanely in accordance with the guidelines on animal experimentation of our institute and the Position of the American Heart Association on Research Animal Use. All protocols were approved

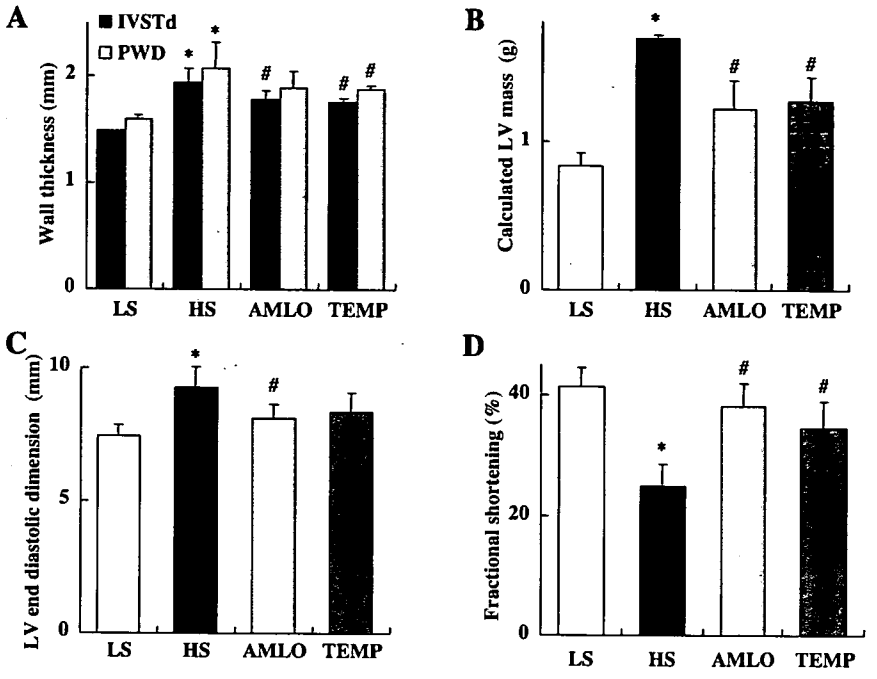

Fig. 2. *The results of echocardiography of DS rats at 17 weeks. A: The wall thickness of IVSTd and PWTd of LV of LS, HS, AMLO and TEMP rats at 17 weeks* (n = *10, 5, 6, 4, respectively). B: The calculated LV mass of LS, HS, AMLO and TEMP rats at 17 weeks* (n = *10, 5, 6, 4, respectively). C: The LVDd of LS, HS, AMLO and TEMP rats at 17 weeks* (n = *10, 5, 6, 4, respectively). D: The fractional shortening of LS, HS, AMLO and TEMP rats at 17 weeks* (n = *10, 5, 6, 4, respectively). Data are expressed as the mean ± SEM.* *$p < 0.05$ vs. *LS rats.* #$p < 0.05$ vs. *HS rats.*

by the Institutional Animal Care and Use Committee of Chiba University Graduate School of Medicine.

Echocardiography

The LV dimension, contraction, LV wall thickness, and LV fractional shortening (FS) were determined by echocardiography after anesthesia with an intramuscular injection of pentobarbital sodium (15 mg/kg BW). Transthoracic echocardiography was performed at the ages of 6, 11, and 17 weeks in all rats using an HP Sonos 5500 (Hewlett-Packard Co., Andover, USA) with a 10-MHz imaging linear scan probe transducer as described previously (*25*, *26*).

Histological Analysis

The heart was weighed, then fixed by perfusion with 3.8% formaldehyde, embedded in paraffin, sectioned into 4 μm slices, and stained with hematoxylin-eosin (H-E) or van Gieson stain (*25*). To determine the degree of collagen fiber accumulation, we selected 10 fields at random and calculated the ratio of the fibrotic area by van Gieson staining to the total myocardial area by using NIH IMAGE software (NIH Research Service Branch, Bethesda, USA) (*25*). Apoptosis was detected by *in situ* terminal deoxynucleotidyl transfer-mediated end labeling of fragmented nuclei (TUNEL assay) using an *in situ* apoptosis detection kit (CardioTACS™; TREVIGEN Inc., Gaithersburg, USA) according to the supplier's instructions. The oxidation of the myocardium was determined by immunostaining using anti–4-hydroxy-2-nonenal antibody (anti-4-HNE; ALEXIS Biochemicals, USA) reacted with avidin-conjugated peroxidase (VECTASTAIN ABC kit, VECTOR, Burlingame, USA), and visualized with 3,3′-diaminobenzidine (Peroxidase substrate kit DAB, VECTOR). For semiquantification, the area and the intensity of 4-HNE staining were scored as reported previously (*27*). A part of the LV was frozen at −80°C for mRNA analysis.

RNA Preparation and DNA Microarray Analysis

Total RNA was isolated from rat heart ventricles using the lithium/urea method and separated on a 1.0% agarose/formaldehyde gel. cDNA of brain natriuretic peptide (BNP) was labeled by a random priming method with [α-^{32}P]dCTP and hybridized to membranes as described previously (*25*). An RNase protection assay (using 20 μg of total RNA) was performed using a rat cytokine Multi-Probe Template Set (BD Pharmingen Bioscience, San Jose, USA) according to the

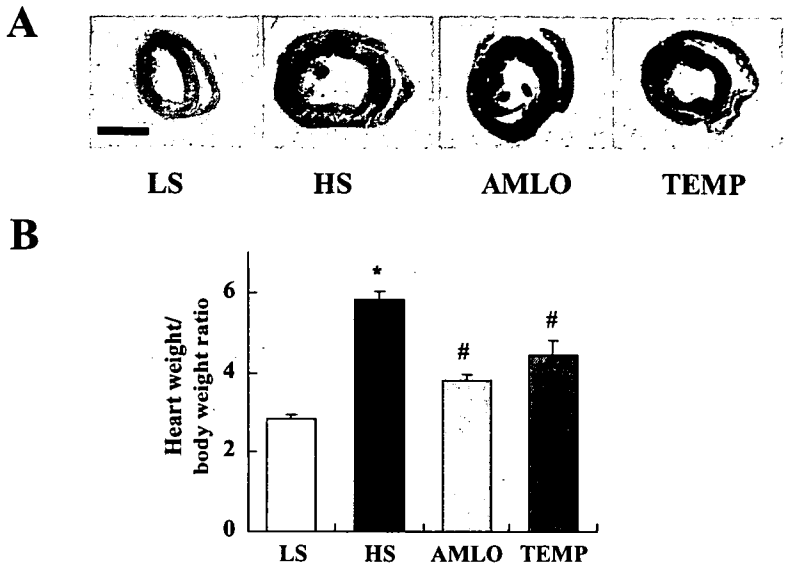

Fig. 3. *The heart-weight-to-body-weight ratio of DS rats at 17 weeks. A: H-E staining of the heart of LS, HS, AMLO and TEMP rats at 17 weeks* (n = *10, 5, 6, 4, respectively). The bar indicates 5 mm. B: The heart-weight-to-body-weight ratio of LS, HS, AMLO and TEMP rats at 17 weeks* (n = *10, 5, 6, 4, respectively). Data are expressed as the mean±SEM.* *p < *0.05* vs. *LS rats.* #p < *0.05* vs. *HS rats.*

manufacturer's instructions (*25*). Hybridized bands were quantified with a FUJIX Bio-Imaging Analyzer BAS 2000 (Fuji Film Co., Tokyo, Japan). Polyadenylate [poly(A)+] RNA was purified from the total RNA with a QuickPrep mRNA purification kit (Pharmacia Biotech, Piscataway, USA). The experimental procedures for the gene chip analysis were performed according to the Affymetrix GeneChip Expression Analysis Technical Manual (Affymetrix, Santa Clara, USA) (*28–30*). The Affymetrix GeneChip U34A set was derived from selected genes and ESTs from the 18 November 1998 release of Genbank. Each 8800 gene is represented on the arrays by perfectly matched 25-mer (PM) oligonucleotides and mismatched (MM) 25-mer control probes that are identical except for one base. The expression levels were calculated by background-subtracting the hybridization signal of MM from its PM partner and averaging the difference for the probe pair set for individual genes. The RNA levels of each gene were scanned and scored for which the computer algorithm (Affymetrix) returned a "present" call. All calculations were performed by Affymetrix software (*31*). The data were analyzed by the program FileMaker Pro 4.0 for Macintosh. Among the 8,800 clones included in the gene chip analysis, we selected those genes having an intensity of >100. Among these genes, we picked out ratio values >1.7 or <−1.7 as indicating genes with changed expression.

Statistical Analysis

All data are expressed as the mean±SEM of 3–4 independent experiments. Mean differences among the 4 groups were tested by one-way ANOVA followed by Scheffe's modified *F*-test for multiple comparisons. Comparisons of follow-up body weight, blood pressure, pulse rate and echocardiographic data were tested using repeated measure ANOVA followed by Scheffe's modified *F*-test. Values of $p<0.05$ were considered statistically significant.

Results

Development of Cardiac Hypertrophy and Heart Failure in Dahl Salt-Sensitive Rats

A loss of body weight was observed in HS rats, but the treatment with amlodipine significantly attenuated it (Fig. 1A). The initial systolic BP (SBP) at 6 weeks of age was 108.5±11.4 mmHg (mean±SEM, $n=34$). SBP was gradually increased, reached a level of over 200 mmHg by 11 weeks, and remained over 200 mmHg thereafter in HS rats. The SBP was not decreased in AMLO or TEMP rats and there was no significant difference in SBP among HS, AMLO and TEMP rats (Fig. 1B). At the age of 14–16 weeks, all HS rats lost BW and displayed rapid and labored respiration characteristic of CHF, and by 17 weeks, 5 of 10 rats had died. On the other hand, all LS rats were alive without any symptoms and 6 of 7

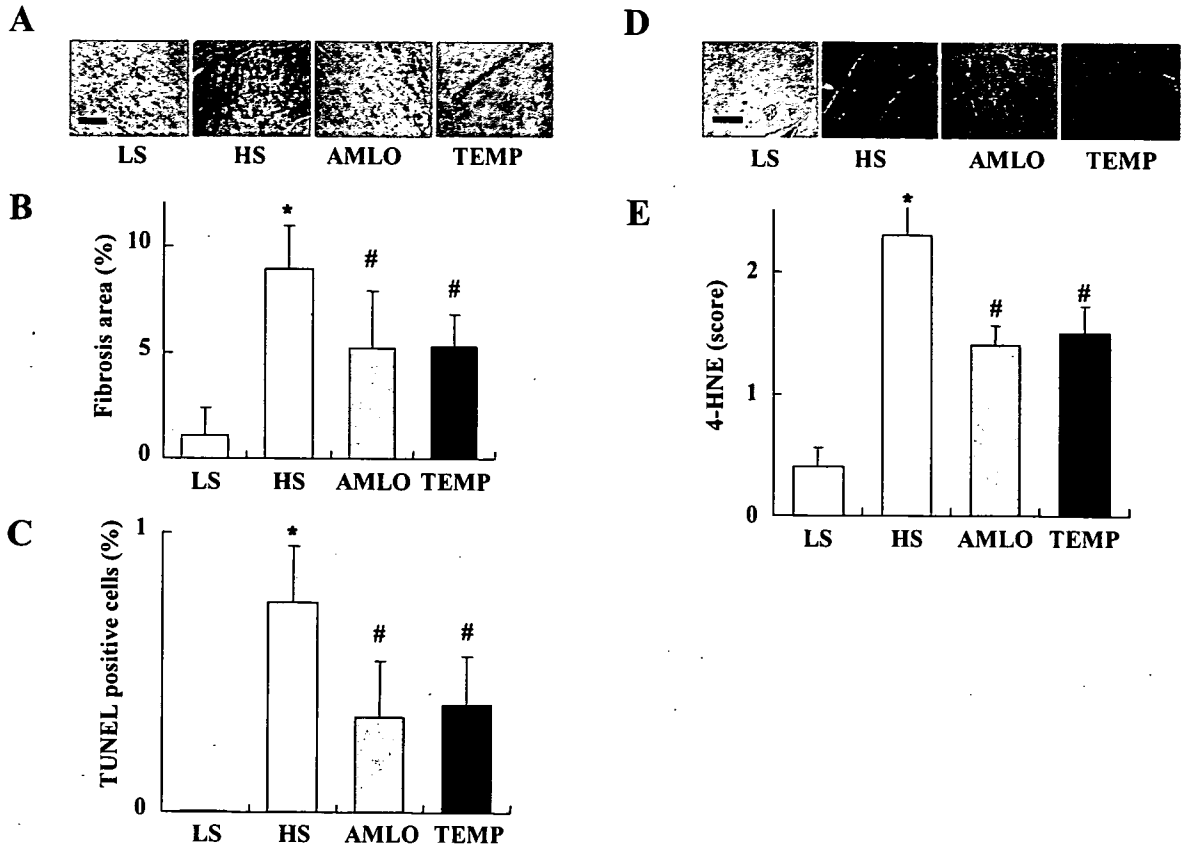

Fig. 4. *The fibrosis and apoptosis of DS rats. A: Representative photographs of von Gieson staining of the heart of LS, HS, AMLO and TEMP rats at 17 weeks. The bar indicates 100 μm. B: The percentage of fibrotic area in the heart of LS, HS, AMLO and TEMP rats at 17 weeks* (n = *10, 5, 6, 4, respectively). C: The percentage of TUNEL-positive cells in the heart of LS, HS, AMLO and TEMP rats at 17 weeks* (n = *10, 5, 6, 4, respectively). D: Representative photographs of 4-HNE staining of the heart of LS, HS, AMLO and TEMP rats at 17 weeks. The bar indicates 100 μm. E: The scoring of the staining of 4-HNE of the heart of LS, HS, AMLO and TEMP rats at 17 weeks* (n = *10, 5, 6, 4, respectively). Data are expressed as the mean ± SEM.* *$p < 0.05$ vs. *LS rats.* #$p < 0.05$ vs. *HS rats.*

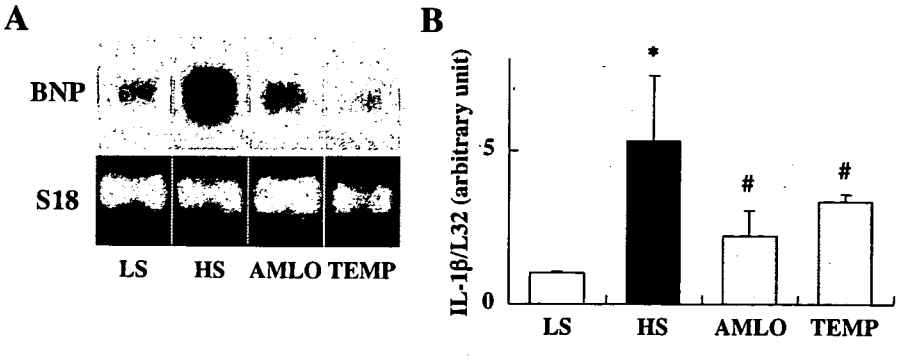

Fig. 5. *The gene expression of DS rats. A: Representative photograph of the expression of BNP using Northern blot analysis. B: The expression of IL-1β of LS, HS, AMLO and TEMP rats at 17 weeks determined by RNase protection assay. Data are expressed as the mean ± SEM.* *$p < 0.05$ vs. *LS rats.* #$p < 0.05$ vs. *HS rats.*

Table 1. The List of Genes Increased in HS and Decreased in AMLO and TEMP Rats Heart

	HS/LS	AMLO/HS	TEMP/HS	Accession No.
Cell division				
Rat mRNA for cdc25B, complete cds	2.9	−4.6	−1.8	D16237
Cyclin D1	1.8	−2.3	−2.1	D14014
Cell signaling				
Arachidonate 12-lipoxygenase	217.9	−231.6	−226.8	L06040
Pancreatitis-associated protein	51.3	−17.7	−3.3	M98049
Cell adhesion molecule, neural (CD56)	18.3	−12.4	−5.4	AI137246
Neuron specific protein PEP-19 (Purkinje cell protein 4)	14.8	−14.3	−13.9	M24852
Lysyl oxidase	13.3	−8.9	−6.4	S66184
Arg/Abl-interacting protein ArgBP2	10.6	−2.9	−2.0	AI058393
Rattus norvegicus mRNA Best5 protein	10.2	−3.6	−4.6	Y07704
Fibronectin (cell-, heparin-, and fibrin-binding domains) gene	8.1	−2.1	−1.7	L00191
Carbonic anhydrase II gene	8.1	−7.7	−6.8	U60578
Sialoprotein (osteopontin)	7.0	−3.7	−2.0	M14656
Rattus norvegicus mRNA Best5 protein	6.6	−2.9	−3.8	Y07704
Rattus norvegicus protein kinase C-binding protein Enigma mRNA	5.3	−4.7	−2.9	U48247
Isk protein	5.0	−6.0	−2.7	D10709
Prostaglandin F2α receptor	5.0	−3.3	−1.7	S74898
GATA-binding protein 4	5.0	−2.7	−2.1	L22761
Calcium channel, voltage-dependent, T type, α1G subunit	4.0	−4.1	−2.0	AF027984
Transforming growth factor-β stimulated clone 22	3.9	−3.4	−1.8	L25785
Follistatin-related protein precursor	3.7	−2.4	−1.8	AA849769
Taurine/β-alanine transporter	3.6	−2.7	−2.0	M96601
S100 Ca-binding protein A4	3.6	−3.2	−2.1	X06916
N^G,N^G-Dimethylarginine dimethylaminohydrolase	3.6	−3.1	−2.4	AA894273
Lipocortin V	3.3	−2.4	−2.2	AF051895
Vesicle-associated membrane protein 5	3.0	−2.5	−1.7	AF054826
Solute carrier family 4, member 1, anion exchange protein 1 (kidney band 3)	2.8	−2.7	−2.8	AA866414
Cadherin 2, type 1, *N*-cadherin (neuronal)	2.7	−2.1	−1.7	AF097593
Muscle Y-box protein YB2	2.7	−2.9	−2.2	D28557
Cerebellar Ca-binding protein, spot 35 protein	2.5	−2.6	−2.2	M31178
Rhesus blood group	2.3	−2.4	−1.8	AB015191
Galectin-5	2.3	−3.3	−2.2	L21711
Immediate-early serum-responsive JE gene	2.2	−1.7	−1.8	X17053
Enolase 1, α	2.1	−1.9	−1.7	X02610
Prolyl endopeptidase	2.1	−5.5	−2.4	AB012759
Glutathione-S-transferase, mu type 2 (Yb2)	2.0	−1.7	−2.1	J02810
Cyclic protein-2=cathepsin L proenzyme	2.0	−2.5	−2.8	S85184
ASM15	2.0	−2.3	−1.8	X59864
Glycogenin	2.0	−1.9	−1.7	U96130
Rat VL30 element mRNA	1.9	−2.2	−1.7	M91234
Adenylyl cyclase–associated protein 2	1.8	−2.0	−1.8	AI145367
Ezrin	1.8	−1.8	−1.7	X67788
Cell structure				
Fast myosin alkali light chain	9.5	−8.0	−2.1	L00088
Rattus norvegicus α-globin (GloA) gene, complete cds	4.9	−7.5	−2.5	AI178971
Ribosomal protein L3	2.7	−2.1	−1.7	X62166
Transthyretin (prealbumin, amyloidosis type I)	2.4	−2.3	−2.2	AA945169
Metabolism				
Aminolevulinate synthase 2, δ	6.7	−9.5	−3.7	D86297
Phosphofructokinase C	4.9	−3.2	−2.0	L25387
Ornithine decarboxylase antizyme inhibitor	2.8	−1.7	−1.8	AI043631

Table 1. (Continued)

	HS/LS	AMLO/HS	TEMP/HS	Accession No.
Unclassified				
ESTs				
ESTs, highly similar to G0S2 MOUSE PUTATIVE LYMPHOCYTE G0/G1 SWITCH PROTEIN 2	22.2	−2.4	−5.2	AA893235
ESTs	16.9	−16.4	−2.4	AA894092
ESTs, weakly similar to T14355 protein-tyrosine-phosphatase [R. norvegicus]	5.4	−6.7	−2.1	AA800303
ESTs, highly similar to 60S RIBOSOMAL PROTEIN L3 [R. norvegicus]	3.8	−2.7	−1.8	AA892367
ESTs	2.5	−3.4	−2.9	AA944361
ESTs	1.9	−2.4	−2.8	H31625

HS/LS, the fold change the gene expression of HS to LS rat; AMLO/HS, the fold change the gene expression of AMLO to HS rat; TEMP/HS, the fold change the gene expression of TEMP to HS.

AMLO rats and 4 of 7 TEMP rats were alive at 17 weeks (Fig. 1C).

Echocardiography

We assessed cardiac geometry and function by echocardiography. In accordance with the increase of SBP, LV wall thickness was increased in HS rats at 17 weeks compared to LS rats (Fig. 2A). The diastolic interventricular septum wall thickness (IVSTd) was significantly thinner in AMLO and TEMP rats than in HS rats (Fig. 2A). The calculated LV mass was increased in HS rats, and treatment with either amlodipine or Tempol reduced it (Fig. 2B). In parallel with the progression of the symptoms of heart failure, LV was dilated (Fig. 2C) and the contraction was impaired (Fig. 2D) in HS rats compared with LS rats. The treatment with either amlodipine or Tempol significantly attenuated the development of LV hypertrophy and dilatation, and improved contraction (Fig. 2A–D).

Histopathology of the Heart

HS rats developed remarkable cardiac hypertrophy compared with LS rats (the weights of the hearts of 17-week-old animals were as follows: LS, 1.25±0.02 mg; HS, 1.84±0.09 mg; AMLO, 1.56±0.12 mg; TEMP, 1.48±0.09 mg; HS *vs.* AMLO, $p<0.05$; HS *vs.* TEMP, $p<0.05$). The heart-weight-to-body-weight (H/B) ratios of the 17-week-old animals were as follows: LS, 2.82±0.14; HS, 5.82±0.20 ($p<0.05$) (Fig. 3). The increase in the H/B ratio was attenuated significantly in the AMLO group and TEMP group compared with the HS group (AMLO, 3.78±0.16, $p<0.05$ *vs.* HS; TEMP, 4.42±0.40, $p<0.05$ *vs.* HS) (Fig. 3). Marked cardiomyocyte hypertrophy and interstitial fibrosis were observed in the LV tissue of 17-week-old HS rats compared to LS rats (Fig. 4A). Quantitative analysis of myocardial fibrosis using van Gieson staining of the heart tissue revealed that the treatment with either amlodipine or Tempol significantly reduced the fibrotic area compared to that in HS rats (LS, 1.1±1.3%; HS, 8.9±3.9%; AMLO, 5.2±2.7%; TEMP, 5.3±1.5%; HS *vs.* AMLO, $p<0.05$; HS *vs.* TEMP, $p<0.05$) (Fig. 4B). Apoptosis has been reported to be involved in the pathophysiology of the development of heart failure in DS rats (*32*). The number of apoptotic cells was increased in HS rats compared to LS rats, but the treatment with either amlodipine or Tempol significantly reduced the number of apoptotic cells detected by the TUNEL method (Fig. 4C). Since the staining score of 4-HNE (a by-product of lipid peroxidation and an indicator of oxidative stress) of the myocardium was increased in HS hearts compared to LS hearts, it was improved in AMLO and TEMP hearts (Fig. 4D, E).

Effects of Amlodipine Treatment on Gene Expression

The mRNA levels of brain natriuretic peptide (BNP) and interleukin (IL)-1β were significantly higher in HS rats compared to LS rats, as reported previously (*33*), indicating that this model of hypertensive heart failure was reliable. The treatment with either amlodipine or Tempol significantly reduced the expression levels of BNP (Fig. 5A) and IL-1β (Fig. 5B) genes. Other myocardial gene expression profiling results were obtained from the gene chip analysis of RNA samples from the hearts of each group. Upregulations of the natriuretic peptide factor precursor A (ANF), BNP, c-fos, β-myosin heavy chain (β-MHC) and Egr-1 genes (data not shown), all of which are known to be upregulated in CHF, were detected by the gene chip, suggesting the reliability of the RNA expression analysis. Since both amlodipine and Tempol significantly inhibited the transition of LV hypertrophy to heart failure, we compared the gene expression profile of each heart treated with either amlodipine or Tempol using a gene chip. Amlodipine treatment changed the expression of 195 genes, and some of these genes may be involved in the beneficial effects of amlodipine on heart failure. Among these 195 genes, 110 genes were increased in HS rats and decreased in AMLO rats. And of these 110 genes, 54 genes were also decreased in TEMP rats (Table 1). Eighty-five genes were

Table 2. The List of Genes Decreased in HS and Increased in AMLO and TEMP Rats Heart

	HS/LS	AMLO/HS	TEMP/HS	Accession No.
Cell signaling				
Aquaporin 7	−42.9	31.7	12.4	AB000507
D site albumin promoter binding protein	−28.4	4.6	17.8	J03179
Mitogen activated protein kinase kinase 2	−12.5	12.2	4.8	L14936
ATPase, Na^+K^+ transporting, α2 polypeptide	−7.2	5.0	4.1	AI177026
Retinoid X receptor γ	−6.2	4.7	2.4	AF016387
A-raf	−5.7	3.1	2.0	X06942
Putative G protein–coupled receptor (SENR) gene	−5.5	6.5	4.2	AB012210
Protein tyrosine phosphatase, non-receptor type 16	−4.9	2.6	2.2	U02553
MHC class II gene	−4.3	3.8	3.5	D45240
Ras-related rab1B protein	−4.1	3.5	3.6	X13905
Pyruvate dehydrogenase kinase, isoenzyme 4	−4.1	4.4	2.8	AF034577
ORF mRNA	−4.0	5.3	4.5	L41685
Guanidinoacetate methyltransferase	−3.9	3.2	1.8	X08056
Dynorphin gene	−3.5	4.4	5.0	M32783
Glycerol-3-phosphate acyltransferase	−3.3	4.2	1.9	U36773
Cytochrome b5	−3.1	2.1	3.3	AA945054
CD74 antigen	−2.7	2.7	2.4	X13044
α-2-Macroglobulin gene exon 1	−2.6	2.6	2.8	X13983
Rat mRNA for pulmonary surfactant-associated protein SP-B	−2.5	2.5	1.8	AI170380
Vitronectin	−2.5	2.2	1.7	U44845
Short chain acyl-coenzyme A dehydrogenase	−2.4	1.9	1.7	J05030
Secretin receptor	−2.2	2.0	1.7	X59132
Short isoform growth hormone receptor	−2.1	2.4	2.0	S49003
Small heterodimer partner homologue	−1.9	1.7	2.0	D86745
Olfactory neuron-specific (clone 50.06, promoter)	−1.9	1.8	1.9	S64924
Ptk-3L=radiation-induced gene	−1.9	1.9	2.3	S77585
Rat mRNA for MHC class II antigen RT1.B-1 β-chain	−1.7	1.8	2.3	X56596
Cell structure				
Myosin, heavy polypeptide 9, non-muscle	−3.0	3.9	2.9	U31463
Metabolism				
Carboxylesterase 1	−5.6	7.0	5.0	L46791
Rattus norvegicus serine protease gene, complete cds	−2.1	2.0	2.0	L38482
Unclassified				
ESTs				
ESTs, weakly similar to T17307 hypothetical protein DKFZp566O084.1	−16.8	13.3	6.6	AI639268
ESTs, highly similar to JN0873 immunophilin p59-mouse	−12.5	12.6	7.3	AI136977
ESTs, highly similar to NUIM_HUMAN NADH-UBIQUINONE OXIDOREDUCTASE 23 kD SUBUNIT PRECURSOR	−4.8	3.8	2.8	AA799479
ESTs, moderately similar to 60S RIBOSOMAL PROTEIN L3	−3.6	3.0	2.1	AA891037
ESTs	−3.4	3.5	2.3	AI009098
ESTs, weakly similar to T13607 hypothetical protein EG:87B1.3-fruit fly	−2.8	2.1	1.7	AI639504
ESTs, highly similar to ROA2 MOUSE HETEROGENEOUS NUCLEAR RIBONUCLEOPROTEINS A2/B1	−2.6	2.5	1.7	AA799511
ESTs	−2.1	1.8	1.9	AA800298

HS/LS, the fold change the gene expression of HS to LS rat; AMLO/HS, the fold change the gene expression of AMLO to HS rat; TEMP/HS, the fold change the gene expression of TEMP to HS.

decreased in HS rats and increased in AMLO rats. Of these 85 genes, 38 genes were also increased in TEMP rats (Table 2). The genes that changed in a similar fashion in both AMLO and TEMP rats may have been involved in the antioxidative mechanisms of amlodipine on hypertensive heart failure. Fibrosis-related genes (arachidonate 12-lipoxygenase, trans-